LANGMUIR Article
Cite This: Langmuir 2019, 35, 9546−9553
pubs.acs.org/Langmuir

Evaporation-Induced Wetting Transition of Nanodroplets on Nanopatterned Surfaces with Concentric Rings: Surface Geometry and Wettability Effects

Shan Gao,[†] Jing Long,[‡] Wei Liu,*[,†] and Zhichun Liu*[,†]

[†]School of Energy and Power Engineering, Huazhong University of Science and Technology (HUST), 1037 Luoyu Road, Wuhan 430074, China

[‡]Wuhan National Laboratory for Optoelectronics, Huazhong University of Science and Technology (HUST), 1037 Luoyu Road, Wuhan 430074, China

Supporting Information

ABSTRACT: Droplet evaporation is widespread in natural and industrial application, and the rapid and efficient evaporation can significantly improve energy efficiency. However, the fundamental mechanism of contact line dynamics and the microscopic characteristics of evaporating nanodroplets are not well understood. Moreover, how to design a nanostructure surface to enhance nanodroplet evaporation remains unclear. Here, through molecular dynamics simulation, we investigated the evaporation dynamics of nanodroplets on various nanoring surfaces with different geometric parameters and wettability. By measuring the changes of contact radius and contact angle, the results showed that nanodroplets successively exhibit constant contact angle (CCA), constant contact radius (CCR), and mix mode during evaporation, and the evaporation-induced CCA−CCR transition, in essence, is a Cassie−Wenzel wetting transition, whose onset time is remarkably dependent on the surface roughness and wettability. We found that this evaporation-induced wetting transition is postponed on the surface with small nanostructure spacing and weak hydrophilicity, and the evaporation rate of nanodroplets improves accordingly. The dense and hydrophobic nanostructures can not only restrain the Cassie−Wenzel transition, but also enhance the evaporation rate of nanodroplets. Last, through the potential energy field analysis of nanoring substrates, we revealed that the Cassie−Wenzel wetting transition of nanodroplets is a process of molecule migration to low potential energy regions. Our work provides guidance for designing nanostructure surfaces to effectively control the droplet wetting state and enhance its mass transfer performance of phase change.

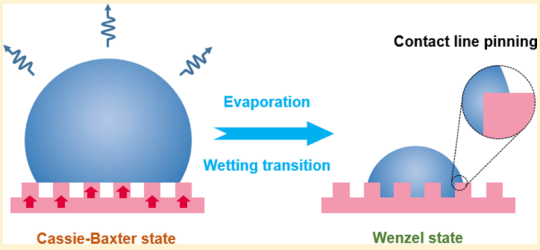

INTRODUCTION

The evaporation of droplets, as a pervasive phenomenon of natural processes, is of great interest and plays an important role in various industrial applications, such as inkjet printing,[1] phase change heat transfer,[2−4] and microfluidic devices.[5−8] Hence, there have been extensive studies on this physical phenomenon over past few decades.[2−4,9−14] In particular, because of the characteristic properties of superhydrophobic surfaces, droplet evaporation dynamics on micro−nano structured surfaces is an active research area and has lately received significant attention.[15−24] Most investigations concentrated on the droplet evaporation patterns,[9,14,25,26] including constant contact angle (CCA), constant contact radius (CCR), and mixed mode (the coupling mode of CCA and CCR), which are influenced by the heat and mass exchange of liquid droplets with the surrounding phase,[27] the physicochemical properties of surface,[10,12,13] and the motion of the triple-phase contact line.[13,14,22,23] Understanding the contact line dynamics is critical to govern the complicated dynamic behavior of evaporating droplets. In the CCA evaporation mode, because of the mobile contact line, the contact angle remains constant and the contact radius decreases with time. For the CCR evaporation mode, the triple-phase boundary is pinned to the surface roughness, leading to a fixed contact radius and a decreasing contact angle. Recent studies indicated that wetting state transitions of droplets occur at the late stage of evaporation.[13,28] When the evaporating droplet shrinks to a small enough size, the suspended Cassie state can be switched to the immersed Wenzel state, along with a strong pinning of the contact line. By contrast, the suspended Cassie state is more desirable because of its excellent mobility;[16,29] thus, it is worthwhile to devote much effort to inhibit the Cassie−Wenzel transition. Unfortunately, the strategy of controlling wetting transition for evaporating droplets is still elusive, and the mechanism of pinning and depinning behaviors of triple-phase contact line has not been revealed much. Furthermore, despite extensive progress, most studies focus on the droplet evaporation dynamics at micron scale, and the dynamic behavior and

Received: June 8, 2019
Published: June 25, 2019

Downloaded via HUAZHONG UNIV SCIENCE & TECHNOLOGY on September 6, 2019 at 10:51:31 (UTC).
See https://pubs.acs.org/sharingguidelines for options on how to legitimately share published articles.

 © 2019 American Chemical Society
DOI: 10.1021/acs.langmuir.9b01731
Langmuir 2019, 35, 9546−9553

micromorphologic change of evaporating nanodroplet remain relatively less understood because of the challenge of experiment observations. Gratifyingly, molecular dynamics (MD) simulation, as a powerful avenue to investigate nanoscale phenomena, can provide intuitive visualizations and micromorphologic characteristics for evaporating nanodroplets on nanostructured surfaces.

In this paper, we adopt the MD simulation method to study the nanodroplet evaporation dynamics on various nanostructure surfaces. Aiming at enhancing evaporation of droplets, guidance for designing nanostructured surface is provided here. The simulation results visualize the evaporation process and the evaporation mode transition, and we show how the contact line dynamics and evaporation mode transition depend on the surface geometric parameters and wettability and how the Cassie−Wenzel wetting transition governs the evaporation mode transition and the evaporation rate of nanodroplets. Finally, the potential energy field of substrates is provided to analyze the wetting transition from the prospective of molecule migration.

■ MODEL AND METHODOLOGY

All simulations were performed using MD simulation to study the evaporation processes of nanodroplets on a series of nanopatterned substrates with different geometric dimensions and wettability. Figure 1 shows the initial configuration of an

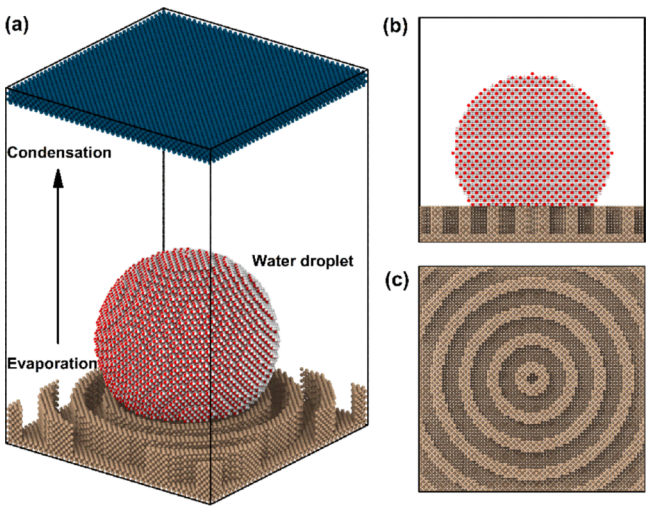

Figure 1. Initial configuration of the simulation system, the nanostructured substrate with concentric rings heats the water droplet to vaporize, and then the gas molecules condense on the upper wall. (a) Orthogonal view of the simulation domain. (b) Vertical section through the droplet. (c) Transverse section through the nanostructured substrate.

evaporating water droplet resting on a nanostructured surface. A spherical-cap droplet with a diameter of 10 nm is meant to be acquired through programming. However, in the actual model, a total of 15 577 water molecules construct the nanodroplet with a diameter of 102.7 Å and an initial contact angle of 120° because of some calculated deviations. The substrates, whose horizontal dimensions correspond to 144.6 Å × 144.6 Å, consist of concentric rings with height H = 18.1 Å, thickness T = 7.2 Å, and a varying interspace S.

To improve the computation efficiency, simpler Cooper-like atoms were used to constitute the real substrates, whose interaction intensity with water molecules, $\varepsilon_{CuO}/\varepsilon_{OO}$, was adjusted to acquire various degrees of surface wettability (see the Supporting Information for an explicit explanation). We examined the dependence of smooth surface wettability on the solid−liquid interaction intensity, and Figure 2 shows the

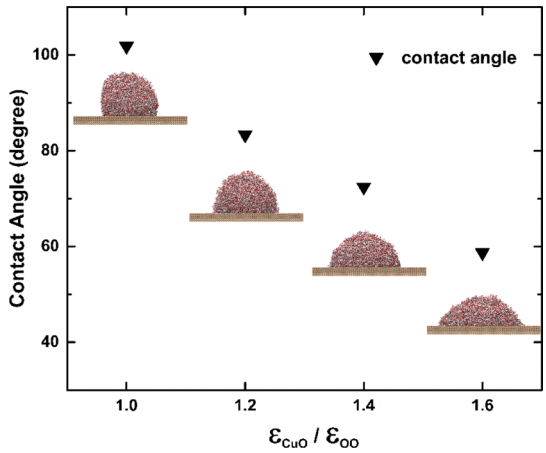

Figure 2. Dependency of the calculated contact angle with respect to the solid−liquid interaction intensity. The insets show the corresponding equilibrium shape of nanodroplets on surfaces with different solid−liquid interaction intensities.

intrinsic contact angles of nanodroplets on smooth substrates with different wettability. A spherical-cap shape nanodroplet was placed on various surfaces with different solid−liquid interaction intensities. The corresponding values of static contact angle θ_0 in the present study are 101.8°, 83.5°, 72.4°, and 58.7° for smooth surfaces with $\varepsilon_{CuO}/\varepsilon_{OO}$ equal to 1.0, 1.2, 1.4, and 1.6, respectively. The insets illustrate the corresponding morphology of droplets in stable states, showing smooth surfaces with energy parameter ratio $\varepsilon_{CuO}/\varepsilon_{OO}$ values of 1.0, 1.2, 1.4, and 1.6 from left to right. As the solid−liquid interaction intensity gradually increases, a surface wettability change from hydrophobicity to hydrophilicity is observed. The results suggest that surfaces increasingly possess hydrophilic property when increasing van der Waals interactions exist between the substrate atoms and water molecules.

Both the substrate atoms and water molecules are initially generated in the face-centered cubic lattice, whose lattice constants are determined by their respective density. The hot substrate heats the water droplet to vaporize, and a cold smooth wall is placed on the upper boundary to continuously condense gas molecules and guarantee a relatively stable pressure of vapor phase. A large-scale atomic/molecular massively parallel simulator package was used to conduct all simulations, the model implementation methods are same as those in our previous work,[21,30] and detailed simulation settings can be found in the Supporting Information.

■ RESULTS AND DISCUSSION

Evaporation of Nanodroplets on Nanostructured Surfaces. The evaporation dynamics of nanodroplets on various textured surfaces was investigated here. We first simulated the nanodroplet evaporation on a nanopillared surface, which consists of nanopillars with height H = 18.1 Å, width W = 7.2 Å, and spacing S = 14.5 Å. Figure 3a shows the typical snapshots of the evaporating nanodroplet on the nanopillared surface. Particularly, to study the contact line

DOI: 10.1021/acs.langmuir.9b01731
Langmuir 2019, 35, 9546−9553

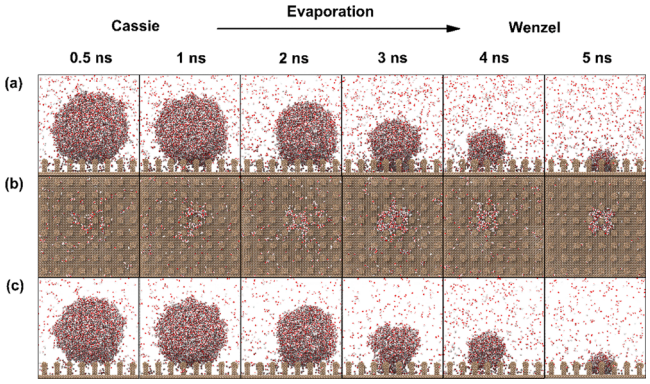

Figure 3. (a) Time-dependent snapshots of the side views of evaporating nanodroplet on the nanopillared surface. (b) Time-dependent snapshots of the transverse section view and (c) snapshots of the vertical section view complementarily revealing the invading dynamics of triple-phase contact line and the Cassie−Wenzel wetting transition induced by evaporation.

dynamics of the evaporating nanodroplet, the snapshots of the transverse section view and vertical section view of the simulation system are correspondingly shown in Figure 3b,c. During the evaporation process, the suspended Cassie droplet gradually impales structure gaps and transforms into an immersed Wenzel state, suggesting an evaporation-triggered wetting transition.

This arresting phenomenon also happens to evaporating nanodroplets on nanopatterned surfaces with concentric rings, as shown in Figure 4a. Furthermore, to investigate the contact line dynamics of evaporating nanodroplets, the snapshots of the transverse section view and vertical section view of the simulation system are correspondingly shown in Figure 4b,c. According to these time-lapse images, the evaporation process of nanodroplets on nanostructured surfaces can be divided into three distinctive regimes. (I) CCA mode: In this early stage, the evaporating nanodroplet is in the Cassie state. The gas molecules trapped in nanostructures marks the inexistence of contact line pinning, the three-phase contact line suspends on surface, and its motion is nearly insusceptible to surface defect, which can be intuitively observed in those sectional views. Therefore, the droplet shrinks as its height decreases, while its contact angle remains approximately constant. (II) CCR mode: From sectional views, it is found that water molecules gradually invade and fill the nanostructures underneath, indicating nanodroplet transformation into a wetted state, namely, a spontaneous evaporation-induced Cassie−Wenzel wetting transition. In this stage, because of the impalement of vapor pockets, the pinned contact line is constrained by the edges of nanotexture, which greatly limits the mobility of the droplet. As a result, the footprint area of the droplet remains constant and the contact angle decreases with time. (III) Mixed mode: When the dynamic contact angle reduces to the critical receding contact angle, the depinning force is enough to overcome pinning force and detach the contact line from structures, causing a coupled process with simultaneously decreasing contact angle and contact line. Detailed definitions of the receding contact angle are explained in Supporting

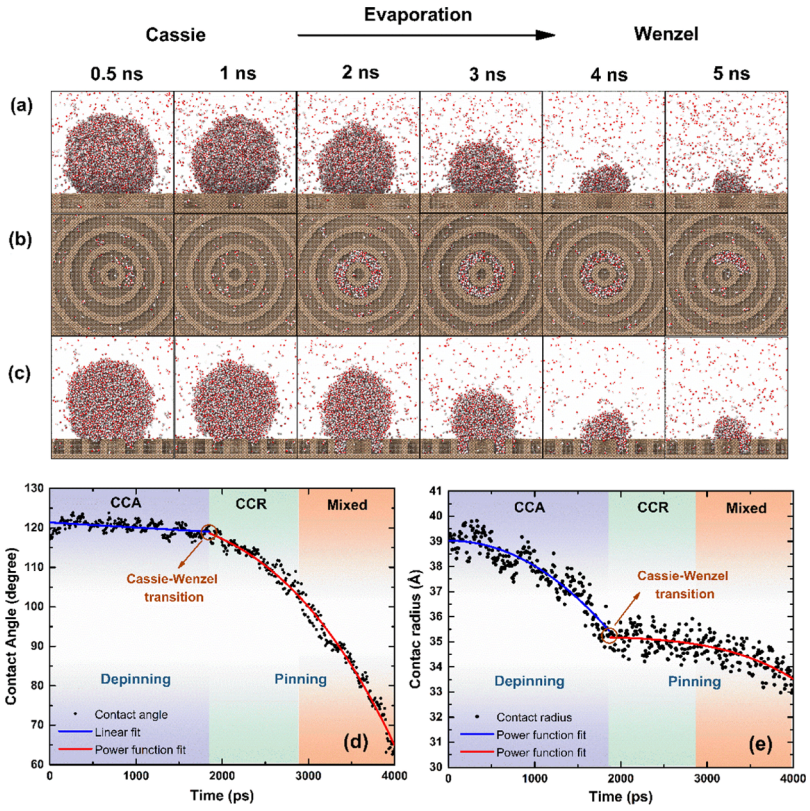

Figure 4. (a) Time-dependent snapshots of the side views of the evaporating nanodroplet on concentric nanorings. (b) Time-dependent snapshots of the transverse section view and (c) snapshots of the vertical section view complementarily revealing the invading dynamics of triple-phase contact line and the Cassie−Wenzel wetting transition induced by evaporation. (d,e) Temporal evolutions of contact angle and contact radius for the evaporating nanodroplet on concentric nanorings.

DOI: 10.1021/acs.langmuir.9b01731
Langmuir 2019, 35, 9546−9553

Information, and the critical receding contact angle in our study is the dynamic angle of the evaporating droplet at the CCR-mixed transition point, whose value can be obtained by recording its temporal evolution (as shown in Figure 4d).

Our simulation results showed that the wetting transition onset time of evaporating nanodroplets on ring nanotextures is within 1−2 ns, which is lower than the 2−3 ns of nanopillared surfaces, because the shrink direction of three-phase boundary is perpendicular to concentric nanorings, representing an interesting case of an extremely strong pinning effect. Thus, the concentric ring nanopatterned surface was selected to study the evaporation dynamics of nanodroplets instead of the common nanopillared surface. The time evolutions of contact angle θ and contact radius R_c are, respectively, demonstrated in Figure 4d,e (see Supporting Information for the detailed calculation method), where these three evaporation stages can be distinguished quantitatively. θ remains roughly constant in the initial receding stage (CCA mode) and gradually decreases in the latter pinning stages. Correspondingly, R_c first decreases in time with a power-law relation (CCA mode), then remains roughly constant (CCR mode), and decreases again in the final combined stage. The criterion of evaporating phase division herein is as follows: the CCA−CCR transition, which is an obvious turning region, can be easily identified by comparing the change rate of R_c between the previous two evaporating mode. The variation patterns of R_c in both CCR mode and mixed mode are fitted using a power function, but R_c remains roughly constant at first, which is the characteristic of CCR mode. Hence, we defined the CCR-mixed transition as the point whose R_c value is reduced by 1% compared with the CCA−CCR transition point, and R_c gradually decreases again in the final combined stage, which is also observed in our visible simulation results.

It is worth noting that, although the contact radius R_c decreases in a power function manner at each stage, its variation rate is immensely disparate and follows the relation: CCA mode > mixed mode > CCR mode, which might be elucidated by analyzing the local forces at triple-phase contact line.[13,31] The depinning force F_D propels the motion of the contact line and can be expressed as

$$F_D = 2R_c\sigma_{LV}(\cos\theta - \cos\theta_C) \quad (1)$$

where R_c is the contact radius of the droplet, σ_{LV} is liquid−vapor surface tension, θ is the dynamic contact angle of the droplet during evaporation, and θ_C is the apparent contact angle on rough surface. Correspondingly, the pinning force F_P hinders contact line movement and is estimated to be

$$\begin{aligned} F_P &= 2R_c\sigma_{LV}(\cos\theta_A - \cos\theta_R) \\ &= 2R_c\sigma_{LV}[(\cos\theta_{A0} - \cos\theta_{R0})\phi + H_r] \end{aligned} \quad (2)$$

where $\cos\theta_A$, $\cos\theta_{A0}$, $\cos\theta_R$, and $\cos\theta_{R0}$ are advancing and receding contact angles for the corresponding rough and smooth surfaces, ϕ denotes the fraction of the solid−liquid contact area ($\phi = 1$ for the Wenzel state and $0 < \phi < 1$ for the Cassie state), and the term H_r is the adhesive force caused by surface roughness. Obviously, the pinning force of the Wenzel droplet is stronger than the Cassie droplet because of the larger solid−liquid contact area fraction. In the binning CCA mode, the droplet suspends on a rough surface and stays in a Cassie state; hence, the weak pinning force prompts the contact line of the evaporating droplet to dramatically shrink. Oppositely, the droplet transforms into an immersed Wenzel state in the following CCR mode, the evident pinning effect causes the contact line to stick to the surface roughness and further results in a diminishing dynamic contact angle (in this stage, F_D keeps increasing but is still smaller than F_P). As the dynamic contact angle further decreases to a critical value, namely, the critical receding contact angle, the evaporating droplet enters into the mixed mode, where F_D overcomes F_P to shrink the contact line again. However, compared with CCA mode, the decrease of the contact radius in mixed mode is sluggish because of the strong pinning effect of the Wenzel state. The cross-over point between CCA mode and CCR mode can be noticed to mark the onset time of Cassie−Wenzel wetting transition, and we found that the substrate geometric parameter and wettability prominently affects the CCA−CCR transition.

Surface Geometry Effect on the Evaporation of Nanodroplets. Keeping the surface wettability and other parameters fixed, evaporation processes on four nanoring surfaces with different structure gaps were simulated and analyzed herein, and these surfaces with an increasing spacing of nanoring S are, respectively, denoted as structure 1, structure 2, structure 3, and structure 4; detailed geometric parameters are listed in Table S2 of Supporting Information. Figure 5a shows selected snapshots of the evaporating nanodroplet in each case, and it is observed that the evaporation-triggered wetting transition is sensitive to the geometric parameters. On surfaces with wider structure spacing, the evaporating droplet is more prone to penetrate into nanostructure gaps and form an immersed Wenzel state when its size is comparable to the scale of nanostructure, which might be explained by analyzing the droplet surface energy before and after the wetting transition.[13] During evaporation, the global surface energies E_C and E_W for the Cassie and the Wenzel states decrease with the decreasing droplet size. When the contact radius is large (in the initial evaporation stage), the Cassie state is energetically favorable with a lower value of E_C than E_W. However, E_W decreases faster than E_C as droplet size shrinks,[28] thus the Cassie−Wenzel transition energy difference $\Delta E = E_C - E_W = 0$ when the decreasing contact radius reaches a critical value, which signals the occurrence of wetting transition. For surfaces with wider structure spacing, the wetting transition energy difference at the initial moment is smaller; as a result, the evaporating droplet can convert into the immersed Wenzel state earlier.

In order to quantitatively evaluate the effects of surface geometry on evaporation dynamics of droplets, we calculated and recorded the contact radius for each case, as shown in Figure 5b. The results indicate that the variation of the contact radius in the CCA stage demonstrates a similar tendency to the power-law function (fitted by the blue line). It is noteworthy that the onset time of Cassie−Wenzel wetting transition for different surfaces follows the relation: structure 1 > structure 2 > structure 3 > structure 4. That is, the Cassie−Wenzel wetting transition or the CCA−CCR transition was gradually promoted when the substrate changes from structure 1 to structure 3, while for structure 4, the nanodroplet immediately wetted the substrate and formed a Wenzel state from the start of evaporation because of the extremely large spacing. Furthermore, we defined evaporated molecules as the water molecules depositing on the upper cold surface (see the inset at the lower right of Figure 5c), whose temporal evolution of the total number is recorded in Figure 5c. For all the nanoring surfaces, there is an increase in the number of evaporated molecules. To observe the variation trend and difference more

DOI: 10.1021/acs.langmuir.9b01731
Langmuir 2019, 35, 9546−9553

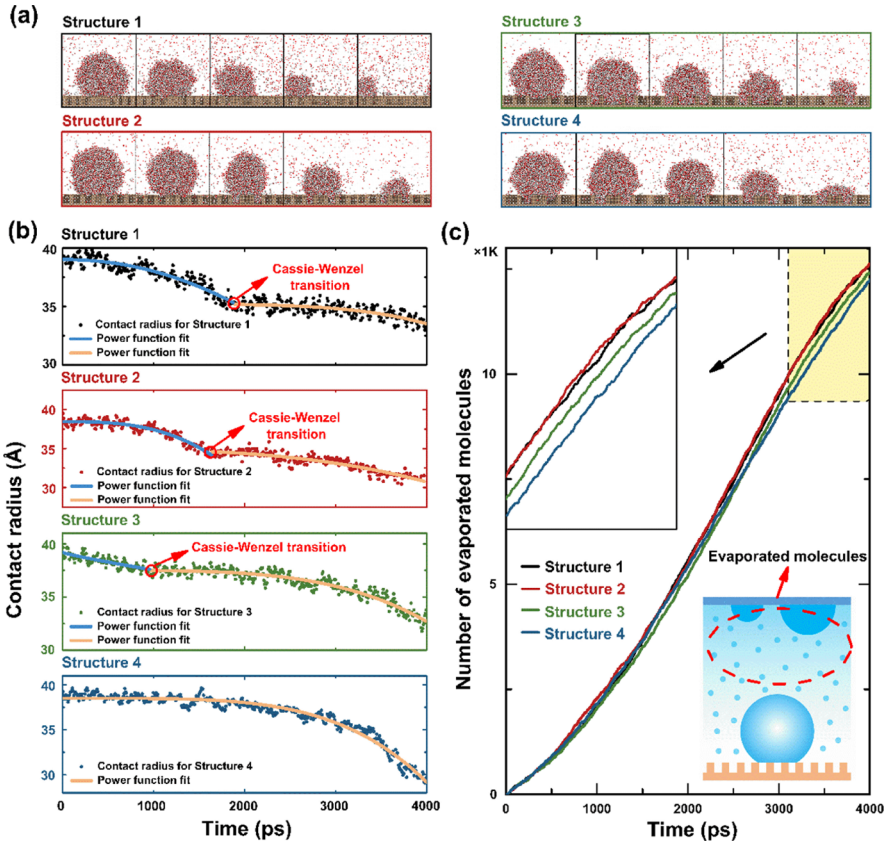

Figure 5. (a) Time-dependent snapshots of the vertical section view of the evaporating nanodroplet on nanoring surfaces with different structure gaps; these surfaces with an increasing spacing of nanoring *S* are, respectively, denoted as structure 1, structure 2, structure 3, and structure 4. (b) Temporal evolution of the evaporating droplet's contact radius on different nanoring surfaces. (c) Temporal evolution of the number of evaporated molecules (molecules deposited on the upper cold surface); the inset at upper left shows the graphic details in large coordinate values.

clearly, details in the final stage are illustrated by the inset at upper left. Clearly, the evaporation rate of each surface follows the relation structure 1 ≈ structure 2 > structure 3 > structure 4, which is roughly consistent with the variation relation of the Cassie−Wenzel transition onset time. Therefore, we can infer that the evaporation rate of the Cassie droplet is higher than the Wenzel state, and the deferred Cassie−Wenzel transition endows the structure 1 with best mass transfer performance during evaporation. Briefly, the smaller the nanostructure spacing, the less favorable it is for Cassie−Wenzel transition, corresponding to a smaller base size of the evaporating droplet at the CCA−CCR transition and a higher evaporation rate of the sessile droplet. Based on the above results, we conclude that properly reducing the structure gap can not only restrain the Cassie−Wenzel wetting transition, but also enhance the mass transfer performance of the nanostructured surface during droplet evaporation.

Surface Wettability Effect on the Evaporation of Nanodroplets. Keeping the surface topography and other parameters fixed, we simulated the evaporation processes on four nanoring surfaces with different wettability; these surfaces with an increasing wettability are denoted as wettability 1, wettability 2, wettability 3, and wettability 4, and the detailed setting parameters are listed in Table S3 of Supporting Information. Figure 6a shows selected snapshots of the evaporating nanodroplet in each case. Obviously, with the enhancement of surface hydrophilicity, the evaporating droplet immersed into structure gaps earlier and formed a wetted state with a smaller contact angle and larger contact radius. Because for surfaces with stronger hydrophilicity, the wetting transition energy difference at the initial moment is smaller, the evaporating droplet can convert into the immersed Wenzel state more easily.

In order to quantitatively verify the aforementioned visualized results, the contact angle was calculated and its variation was recorded in Figure 6b, which was used to analyze the effects of surface wettability on evaporation dynamics of droplet. As we know, the contact angle remains constant in CCA mode, thus, the decrease of the contact angle can be used to mark the change of evaporating mode, namely, the occurrence of CCA−CCR transition. The red dash lines in Figure 6b indicate the onset time of Cassie−Wenzel wetting transition of different surfaces follows the relation: wettability 1 > wettability 2 > wettability 3 > wettability 4. That is, the Cassie−Wenzel wetting transition or the CCA−CCR transition was gradually promoted with the enhancement of substrate hydrophilicity. It should be noticed that the contact angle increases in the initial CCA stage for wettability 1 because of the long-duration energy relaxation of the droplet on this extremely hydrophobic substrate. In addition, we also calculated the number of evaporated molecules, whose temporal evolution is shown in Figure 6c. From the inset at lower right, which illustrates the graphic details in large coordinate values, we found that the evaporation rate of each surface follows the relation wettability 1 ≈ wettability 2 > wettability 3 > wettability 4. We can conclude that improving the surface hydrophobicity not only restrains the Cassie−Wenzel wetting transition (CCA−CCR transition) of the

DOI: 10.1021/acs.langmuir.9b01731
Langmuir 2019, 35, 9546−9553

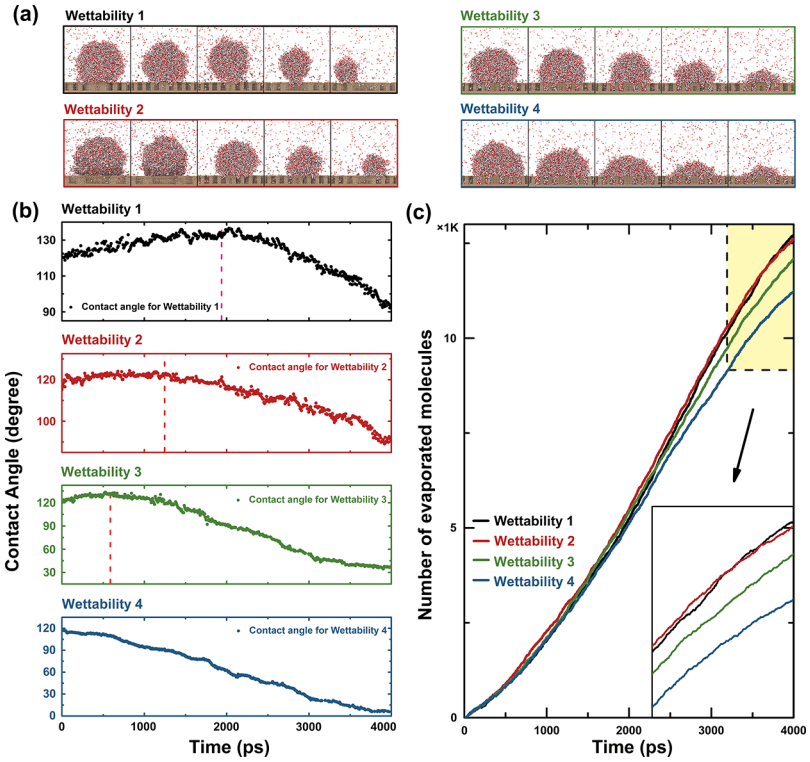

Figure 6. (a) Time-dependent snapshots of the vertical section view of the evaporating nanodroplet on nanoring surfaces with different wettability; these surfaces with an increasing wettability are denoted as wettability 1, wettability 2, wettability 3, and wettability 4. (b) Temporal evolution of the evaporating droplet's contact angle on different nanoring surfaces. (c) Temporal evolution of the number of evaporated molecules (molecules deposited on the upper cold surface), the inset at lower right shows the graphic details in large coordinate values.

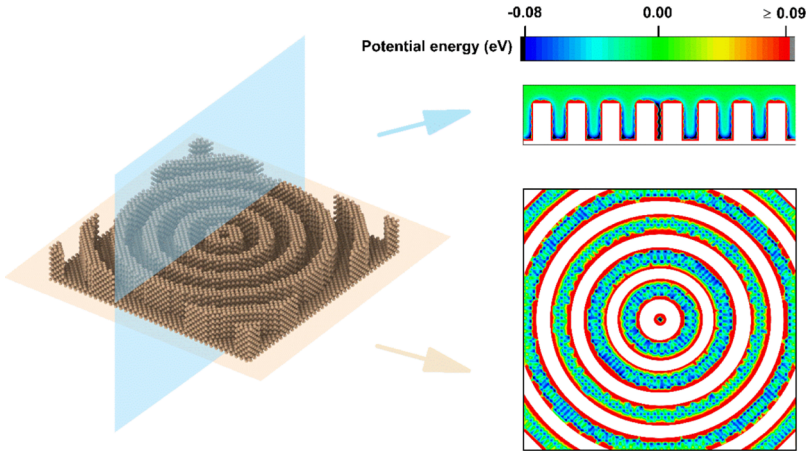

Figure 7. Equipotential curves of potential energy between one water molecule and all substrate atoms for two representative cross sections.

evaporating droplet, but also enhances the mass transfer performance of the nanostructured surface during droplet evaporation.

The aforementioned results reveal that the large structure spacing and strong hydrophilicity of the surface promote the Cassie–Wenzel wetting transition, and its mechanism was analyzed herein from the perspective of potential energy. According to the 12–6 Lennard-Jones potential, we calculated the potential energy between one water molecule and all surface atoms, and a transverse section and a vertical section of surface were selected to plot the contours of potential energy, as shown in the Figure 7. The region in structure gaps possesses a lower potential energy compared with the nanoring top region. As a result, water molecules are inclined to accumulate in the structure gaps when the droplet size is comparable to the scale of nanostructure, yielding an immersed Wenzel droplet. Enlarging the structure spacing increases the proportion of nanostructure gap region with lower potential energy, and enhancing the surface hydrophilicity reduces the potential energy of nanostructure gap region, and both these methods improve the possibility of water infiltration to nanostructure gap and further promote the suspended Cassie state to the immersed Wenzel state wetting transition during droplet evaporation.

DOI: 10.1021/acs.langmuir.9b01731
Langmuir 2019, 35, 9546–9553

CONCLUSIONS

In summary, on various nanostructure surfaces, the evaporation process and the contact line dynamics of nanodroplets were studied numerically using the MD simulation. For different nanostructure surfaces, we found the evaporation mode transforms in a similar regime: nanodroplets successively exhibits CCA, CCR, and mix mode during evaporation. However, compared with normal nanopillar surfaces, the pinning effect of the contact line is more potent on nanoring surfaces, propelling the occurrence of CCA−CCR transition. The evaporation-induced CCA−CCR transition in essence is caused by the Cassie−Wenzel wetting transition, which is a process of molecule migration to the low potential energy region and is dependent on the surface geometry and wettability. There is a lower CCA−CCR transition onset time on surfaces with larger structure spacing or stronger hydrophilicity, leading to a lower nanodroplet evaporation rate. Hence, the dense and hydrophobic nanostructure surface can not only inhibit the Cassie−Wenzel wetting transition (CCA−CCR transition) of the evaporating droplet, but also enhance the mass transfer performance of the nanostructured surface during droplet evaporation. These intriguing findings can provide a microscopic insight into the contact line dynamics of the evaporating nanodroplet, and the control strategy of the droplet wetting state provides guidance for the design of nanostructure surfaces to enhance mass transfer during the phase change process.

ASSOCIATED CONTENT

Supporting Information

The Supporting Information is available free of charge on the ACS Publications website at DOI: 10.1021/acs.langmuir.9b01731.

Simulation details, geometric parameters of nanostructured surfaces, the intrinsic contact angle measurement method, and the definitions of advancing and receding contact angles (PDF)

AUTHOR INFORMATION

Corresponding Authors

*E-mail: w_liu@hust.edu.cn (W.L.).
*E-mail: zcliu@hust.edu.cn (Z.L.).

Notes

The authors declare no competing financial interest.

ACKNOWLEDGMENTS

This project was supported by the National Natural Science Foundation of China (nos. 51736004 and 51776079). The study was performed at the National Supercomputer Center in Tianjin, and the calculations were performed on Tianhe-1(A).

REFERENCES

(1) Kong, X.; Xi, Y.; LeDuff, P.; Li, E.; Liu, Y.; Cheng, L.-J.; Rorrer, G. L.; Tan, H.; Wang, A. X. Optofluidic sensing from inkjet-printed droplets: the enormous enhancement by evaporation-induced spontaneous flow on photonic crystal biosilica. *Nanoscale* **2016**, *8*, 17285−17294.

(2) Zheng, Y.; Ma, X.; Li, Y.; Jiang, R.; Wang, K.; Lan, Z.; Liang, Q. Experimental study of falling film evaporation heat transfer on superhydrophilic horizontal-tubes at low spray density. *Appl. Therm. Eng.* **2017**, *111*, 1548−1556.

(3) Dai, X.; Yang, F.; Yang, R.; Huang, X.; Rigdon, W. A.; Li, X.; Li, C. Biphilic nanoporous surfaces enabled exceptional drag reduction and capillary evaporation enhancement. *Appl. Phys. Lett.* **2014**, *105*, 191611.

(4) Alperen Günay, A. A.; Sett, S.; Oh, J.; Miljkovic, N. Steady Method for the Analysis of Evaporation Dynamics. *Langmuir* **2017**, *33*, 12007−12015.

(5) Zheng, B.; Roach, L. S.; Ismagilov, R. F. Screening of protein crystallization conditions on a microfluidic chip using nanoliter-size droplets. *J. Am. Chem. Soc.* **2003**, *125*, 11170−11171.

(6) Dugas, V.; Broutin, J.; Souteyrand, E. Droplet evaporation study applied to DNA chip manufacturing. *Langmuir* **2005**, *21*, 9130−9136.

(7) Atencia, J.; Beebe, D. J. Controlled microfluidic interfaces. *Nat. Photonics* **2004**, *437*, 648.

(8) Whitesides, G. M. The origins and the future of microfluidics. *Nature* **2006**, *442*, 368−373.

(9) Adera, S.; Raj, R.; Enright, R.; Wang, E. N. Evaporation-induced Cassie droplets on superhydrophobic microstructured surfaces. *Proceedings of the ASME 2012 10th International Conference on Nanochannels, Microchannels Minichannels*, 2012; p 73224.

(10) Miljkovic, N.; Enright, R.; Maroo, S. C.; Cho, H. J.; Wang, E. N. Liquid Evaporation on Superhydrophobic and Superhydrophilic Nanostructured Surfaces. *J. Heat Transfer* **2011**, *133*, 080903.

(11) Dai, X.; Yang, F.; Yang, R.; Lee, Y.-C.; Li, C. Micromembrane-enhanced capillary evaporation. *Int. J. Heat Mass Transfer* **2013**, *64*, 1101−1108.

(12) Chen, X.; Yao, S.; Wang, Z. Evaporation of Condensate Droplets on Structured Surfaces with Gradient Roughness. *J. Heat Transfer* **2015**, *137*, 080903.

(13) Chen, X.; Ma, R.; Li, J.; Hao, C.; Guo, W.; Luk, B. L.; Li, S. C.; Yao, S.; Wang, Z. Evaporation of droplets on superhydrophobic surfaces: surface roughness and small droplet size effects. *Phys. Rev. Lett.* **2012**, *109*, 116101.

(14) Xu, W.; Choi, C.-H. From sticky to slippery droplets: dynamics of contact line depinning on superhydrophobic surfaces. *Phys. Rev. Lett.* **2012**, *109*, 024504.

(15) Gao, S.; Liao, Q.; Liu, W.; Liu, Z. Nanodroplets Impact on Rough Surfaces: A Simulation and Theoretical Study. *Langmuir* **2018**, *34*, 5910−5917.

(16) Dai, X.; Stogin, B. B.; Yang, S.; Wong, T.-S. Slippery Wenzel State. *ACS Nano* **2015**, *9*, 9260−9267.

(17) Dai, X.; Famouri, M.; Abdulagatov, A. I.; Yang, R.; Lee, Y.-C.; George, S. M.; Li, C. Capillary evaporation on micromembrane-enhanced microchannel wicks with atomic layer deposited silica. *Appl. Phys. Lett.* **2013**, *103*, 151602.

(18) Wu, J.; Ma, R.; Wang, Z.; Yao, S. Do droplets always move following the wettability gradient? *Appl. Phys. Lett.* **2011**, *98*, 204104.

(19) Li, J.; Zhou, X.; Li, J.; Che, L.; Yao, J.; McHale, G.; Chaudhury, M. K.; Wang, Z. Topological liquid diode. *Sci. Adv.* **2017**, *3*, No. eaao3530.

(20) Gao, S.; Liao, Q.; Liu, W.; Liu, Z. Self-Removal of Multiple and Multisize Coalescing Nanodroplets on Nanostructured Surfaces. *J. Phys. Chem. C* **2018**, *122*, 20521−20526.

(21) Gao, S.; Liao, Q.; Liu, W.; Liu, Z. Coalescence-Induced Jumping of Nanodroplets on Textured Surfaces. *J. Phys. Chem. Lett.* **2018**, *9*, 13−18.

(22) Encarnación Escobar, J. M.; Dietrich, E.; Arscott, S.; Zandvliet, H. J. W.; Zhang, X.; Lohse, D. Zipping-Depinning: Dissolution of Droplets on Micropatterned Concentric Rings. *Langmuir* **2018**, *34*, 5396−5402.

(23) Armstrong, S.; McHale, G.; Ledesma-Aguilar, R.; Wells, G. G. Pinning-Free Evaporation of Sessile Droplets of Water from Solid Surfaces. *Langmuir* **2019**, *35*, 2989−2996.

(24) Wen, R.; Lan, Z.; Peng, B.; Xu, W.; Yang, R.; Ma, X. Wetting Transition of Condensed Droplets on Nanostructured Superhydrophobic Surfaces: Coordination of Surface Properties and Condensing Conditions. *ACS Appl. Mater. Interfaces* **2017**, *9*, 13770−13777.

DOI: 10.1021/acs.langmuir.9b01731
Langmuir 2019, 35, 9546−9553

(25) Becker, S.; Kohns, M.; Urbassek, H. M.; Horsch, M.; Hasse, H. Static and Dynamic Wetting Behavior of Drops on Impregnated Structured Walls by Molecular Dynamics Simulation. *J. Phys. Chem. C* **2017**, *121*, 12669−12683.
(26) Mazloomi Moqaddam, A.; Derome, D.; Carmeliet, J. Dynamics of Contact Line Pinning and Depinning of Droplets Evaporating on Microribs. *Langmuir* **2018**, *34*, 5635−5645.
(27) Nguyen, T. A. H.; Biggs, S. R.; Nguyen, A. V. Analytical Model for Diffusive Evaporation of Sessile Droplets Coupled with Interfacial Cooling Effect. *Langmuir* **2018**, *34*, 6955−6962.
(28) Tsai, P.; Lammertink, R. G.; Wessling, M.; Lohse, D. Evaporation-triggered wetting transition for water droplets upon hydrophobic microstructures. *Phys. Rev. Lett.* **2010**, *104*, 116102.
(29) Dai, X.; Sun, N.; Nielsen, S. O.; Stogin, B. B.; Wang, J.; Yang, S.; Wong, T.-S. Hydrophilic directional slippery rough surfaces for water harvesting. *Sci. Adv.* **2018**, *4*, No. eaaq0919.
(30) Gao, S.; Liu, W.; Liu, Z. Tuning nanostructured surfaces with hybrid wettability areas to enhance condensation. *Nanoscale* **2019**, *11*, 459−466.
(31) Nosnovsky, M.; Bhushan, B. Biomimetic Superhydrophobic Surfaces: Multiscale Approach. *Nano Lett.* **2007**, *7*, 2633−2637.

DOI: 10.1021/acs.langmuir.9b01731
Langmuir 2019, 35, 9546−9553